Preprint Title	Antimicrobial and biocompatibility properties of Sono-assisted Fe-modified Zeolite Y
Authors	Jesús I. De León Ramirez, Sergio Pérez Sicairos, José R. Chávez Méndez, Perla E. Nuñez Serafin, Vitalii Petranovskii and Víctor A. Reyes Villegas
Publication Date	19 Juni 2026
Article Type	Full Research Paper
Supporting Information File 1	Supplemantary Material.docx; 38.9 KB
ORCID® iDs	Jesús I. De León Ramirez - https://orcid.org/0000-0003-1393-610X; Sergio Pérez Sicairos - https://orcid.org/0000-0002-1244-3015; José R. Chávez Méndez - https://orcid.org/0000-0002-0445-7601; Vitalii Petranovskii - https://orcid.org/0000-0002-8794-0593; Víctor A. Reyes Villegas - https://orcid.org/0000-0001-5358-4837

Antimicrobial and biocompatibility properties of Sono-assisted Fe-modified Zeolite Y

*Jesús I. De León Ramirez [1 *], Sergio Pérez Sicairos [2], José R. Chávez Méndez [3],Perla E. Nuñez Serafin [1], Vitalii Petranovskii [4] Víctor A. Reyes Villegas [3*]*

[1] Facultad de Odontología, Universidad Autónoma de Baja California, Tijuana, Baja California 22263, México

[2]Center for Graduates and Research in Chemistry, National Technological Institute of Mexico, Technological Institute of Tijuana, Tijuana 22000, Mexico

[3] Facultad de Ciencias de la Salud, Universidad Autónoma de Baja California, Tijuana, Baja California 22263, México

[4]Centro de Nanociencias y Nanotecnología, Universidad Nacional Autónoma De México, Ensenada, Baja California 22860, México

Corresponding author: victor.alfredo.reyes.villegas@uabc.edu.mx[*]
Jesus.isaias.deleon.ramirez@uabc.edu.mx[*]

Abstract

Commercial zeolite Y (CBV 500, Y) from Zeolyst International was used in a Fe ion-exchanged form (FeY) for sonochemical modification at 0.5 or 1 % of divalent, trivalent or a 1:1 molar ratio and at a static pH of 5 and 9. The materials underwent four different studies to evaluate antimicrobial activities. Screening in a well-diffusion method incorporated *C. albicans*, *C. neoformans*, *S. aureus*, and *S. mutants* where the disk-diffusion was done for *E. faecalis* in a CHROMagar indicator. The screening by a broth method assessed *E. coli and E. faecalis*. From the screening, FeYII and FeYII/III were selected for a broth microdilution assay for antibacterial (*E. coli and E. faecalis*) and antimycotic activity (*C. albicans*, *C. neoformans)*. For the viability test, L929 fibroblasts were exposed to zeolites Y, FeYII, and FeYII/III at different concentrations for 24 hours. In conjunction with the MTT assay, microscopic images detail the cellular impact of zeolite exposure. Materials tested on agar against clinical pathogens showed no prominent activity, attributed to limited material diffusion. In a broth test, all samples displayed antibacterial activity. FeY0, FeY0.5II, FeY0.5III, FeYII/III, and FeYII/III9 exhibited notable antimicrobial effects against *E. coli*. Selected for further testing, FeYII and FeYII/III demonstrated concentration-dependent bactericidal effects. Against Gram-positive *E. faecalis*, FeYII showed a more significant impact compared to FeYII/III. Testing on CHROMagar with *E. faecalis* indicated no growth inhibition, affirming the need for liquid to activate the biological activity. Antifungal tests yielded limited growth inhibition. While Y and FeYII were non-toxic in mammal fibroblasts, FeYII/III showed some toxicity, emphasizing the need for careful consideration in biological applications.

Keywords: Zeolite Y, Sonoassisted, Antimicrobial Zeolite, Biocompatibility Zeolite

Introduction

The search for antimicrobial materials has gained particular importance in various applications, such as in raw materials for cosmetics and pharmaceuticals, hospital and veterinary products, and food manufacture and animal feeding, among others [1]. Zeolites are a class of crystalline aluminosilicates built from corner-sharing (Si or Al)O_4 tetrahedra structures that follow the Lowenstein rule, forming a well-defined tridimensional reticular microporous framework of cavities and channels/cages for reactant molecules adsorption, transformation, and reaction [2]. These porous materials can occur naturally (where volcanic rocks and ash layers react with alkaline groundwater) and can be synthesized artificially in the laboratory. Until now, the International Zeolite Association (IZA) Structure Commission has reported more than 200 unique zeolite frameworks, and the number is continuously increasing [3].

Many zeolites are biocompatible and non-toxic, which can be edible given their nutritious and antibacterial properties [4]. In addition to the unique features like molecular sieve structure, ionic exchangeability, and water absorbent [5], the highly absorbent to several substances expands the use of these biomaterials in various fields of medical science [4]. The most highlighted medical sciences application of zeolite is in drug delivery systems and absorption/release of several drugs, such as anticancer drugs. The application of zeolite in biomedical sciences is expanding and is expected to grow in the coming decades on account of the development of innovative zeolite-based delivery systems along with the emergence of new classes of therapeutics that require smart delivery systems for their biological activity [4]. Currently, the biotechnologies and medicine applications are the following: protection of the living environment (purification of water, soil and air, including the removal of radioactive contaminants), detoxification of living organisms, agriculture, veterinary medicine and zootechnology, biomolecules and cell types separation, drug and gene delivery, construction of biosensors and detection of biomarkers, creation of novel antioxidants, haemostatics, wound dressings, scaffolds for tissue engineering and implant coatings [6].

Specifically, faujasite has proven useful in drug delivery, wound healing and endocytosis studies [6]. Showing to be biocompatible when evaluating cytotoxicity activity on alveolar epithelial cells (A549), human endothelial cells (EA.hy926), and differentiated macrophages (THP-1) cell lines by mitochondrial activity (MTT) and cell membrane integrity (LDH leakage assay) were reported and demonstrated no significant cytotoxic after 24 h of exposure [7].

Interestingly, faujasite, apart from being biocompatible, can protect from reactive oxygen species (ROS) functioning as an antioxidant on human albumin under in vitro conditions converting within the zeolite void system ROS to water molecules, generating H^+ ions [8]. This antioxidative effect of faujasite has also been used to protect human skin fibroblasts from UV-irradiation-generated ROS from TiO_2 photocatalysts [9].

Due to the fact that FAU structures are biocompatible, some studies have tested this material as an ingredient for medicinal products [4,6,10]. For example, NaY was combined with poly(vinylidene fluoride) for bone tissue engineering, promoting the proliferation of human foreskin fibroblasts and mesenchymal stem cells (MSCs). In addition, stimulating the differentiation of MSCs towards osteoblasts. When this NaY composite was implanted subcutaneously in C57Bl/6 mice, the in-vivo study showed no inflammatory response detected from N-acetyl-β-D-glucosaminidase and NO assays performed in blood plasma [11]. Another study proved that when embedding a polyurethane 3D scaffold with fluorinated zeolite Y crystals, the proliferation activity

of human coronary artery smooth muscle cells and depth of penetration of these was significantly increased compared to the zeolite-free scaffolds [12].

Adding to the biocompatibility of FAU, these can also be used for endocytosis studies, as shown to be internalized by human peripheral dendritic cells, finding correlations with the maturation status of cells from the immune system [13]. FAU can be useful for studying cell endocytosis mechanisms and pathways [6]. This property was used with NaY zeolite loaded with magnetic nanoparticles evaluating the zeolite composite for a T2-MRI contrast enhancer in magnetic resonance imaging (MRI) [14]. Proving once again the versatility of FAU and increasing the interest in NaY magnetic composites as biocompatible and non-toxic. Moreover, the effective cellular internalization of the particles by tumor cells guaranteed a significant accumulation in the tumor site, enough to be detected as a darker contrast in the MRI image [10], raising the interest for studies using this zeolitic structure for biosensing.

Given that FAU is biocompatible and non-toxic, it has also been used for improving drug delivery of poor water solubility molecules. Such as clofazimine, an antibiotic used against a wide spectrum of Gram-positive bacteria (GP), leprosy, and multidrug-resistant cancers [15]. Adding to this drug, FAU has also been used as a carrier for oral delivery of non-steroidal anti-inflammatory drugs that are also poorly water-soluble, such as diclofenac, piroxicam [16], and indomethacin where this last was tested in cultures of the Caco-2 human colorectal adenocarcinoma cell line [17]. From these studies, there is no doubt that zeolite Y can be used for drug encapsulation and delivery, adding that they can be highly cytotoxic in cancer cells by significantly reducing cell viability.

Due to the success of NaY for encapsulating drugs, this zeolite was used for testing for anticancer drugs, serving as a carrier for 5-fluorouracil, doxorubicin and mitoxantrone, evaluated with two human colorectal carcinoma cell lines (HCT-15 and RKO cells). Where the loaded NaY was internalized, significantly decreasing cell viability by realizing into the cytoplasm the anticancer drug, while the pristine, unloaded NaY presented no toxicity to either of the two cancer cell lines [18]. Similar effects on human colon adenocarcinoma Caco2 cells were observed when 5-fluorouracil was encapsulated into porous FAU [19]. Hence, the report of low toxicity for zeolite Y, as the adsorption, release, and cytotoxicity of zeolite Y nanoparticles for the cisplatin, an anticancer medicine, demonstrates that the nano-zeolite did not show toxic effects on MG63 cells and exhibited good biocompatibility [10]. A magnetized FAU has also been used for local anticancer treatment, proving great potential in cancerous cell mortality [20].

Another interesting property of FAU zeolites, especially H–Y, is the selective separation from a mixture of microbial cells by specific absorption, of *E. coli*, *B. subtilis* and *S. aureus* [21]. This absorption has been used to create FAU membranes, which, in their Na^+ form, no effect on bacteria was seen in an agar-diffusive assay in comparison to the bactericidal activity against Gram-negative (GN) *E. coli* when exchanged with Ag NP and the bacteriostatic action when exchanged with Zn^{2+} [22]. These ions are the most popular for antimicrobial actions. Although not as popular, Fe can also serve as an antimicrobial agent, but only at specific conditions. For example, in a study where both zinc and copper ions were exchanged nanostructured FAU presented good diffusion and hence presented antimicrobial activity in a broth microdilution antibacterial susceptibility test against methicillin-resistant Staphylococcus aureus (MRSA), whereas in a micro and nanostructure FAU exchanged with Fe no Fe ion release was observed in hence having no antimicrobial activity below 10 ppm [23].

In another study, a Fe-modified FAU was tested as a filtration unit for removing organic, inorganic and biological contaminants, killing from contaminated water waterborne pathogens, i.e., *S. typhi*, *B. subtilus*, *E. coli*, *S. aureus* and *P. aeruginosa* and decontaminating tap water samples within

30 min [24]. The addition of iron nanoparticles into polylactide films caused inhibition of the growth of microorganisms belonging to different groups in terms of morphological structure (GN and GP bacteria, yeast, and molds). Complete growth inhibition was observed for ZVI nanoparticle contents above 3% (w/w) in the PLA matrix [25]. Mmelesi et al. (2021) conducted a review paper where they exhibited photocatalytic activity against organic pollutants and inhibition of antimicrobial growth of cobalt ferrite nanoparticles. Due to their different applications, they concluded the importance of developing a method to achieve the desired properties of spinel ferrites [26]. Jahangirian et al. (2020) reported that a zeolite/Fe_2O_3 nanocomposite was shown to reduce the viability of human melanoma cells, when evaluating the activity against healthy fibroblasts, no toxic effect was observed [27]. Although iron is not often investigated as an antimicrobial, there is evidence that ferrous iron (Fe^{2+}) released by ion exchange contributes to antimicrobial activity. Iron ions can cause oxidative damage to lipids, proteins, and DNA via Fenton or Haber-Weiss reactions, potentially indirectly generating metal-induced antibacterial activity. Despite the important benefits of antimicrobial zeolites exchanged with Cu^{2+}, Zn^{2+}, or Fe^{2+} ions, there is a lack of comprehensive studies examining the correlation between the innate material properties of zeolite particles, especially nano zeolites, and their antimicrobial efficiency [28]. One way to increase the antimicrobial activity of iron-modified zeolites is by using nano zeolites. Since there is an increase in surface area and nanoscopic dimensions which improve the performance of ion release. The antimicrobial applications of nano zeolites are particularly timely in this era of emerging antibacterial resistance, where the fight to prevent the spread of infection is critical and cannot be fully understood [28]. In the literature, we can find descriptions of the potential bactericidal effect of zero-valent iron (nano-Fe0) nanoparticles in Escherichia coli. The bactericidal effect has been found to be dependent on the size and specific properties of nano-Fe0s. A significant increase in antimicrobial activity has also been observed without oxygen. The activity of nano-Fe0 against Bacillus subtilis, Pseudomonas fluorescens, and Aspergillus versicolor has also been studied. The antimicrobial effect of nano-Fe0 has been demonstrated for P. fluorenscens and B. subtilis. However, GN bacteria were less resistant than GP bacteria [29]. Zeolite Y, functionalized with ferric iron di diethyldithiocarbamate complexes, could trap NO radials in liquids and biological systems, enhancing the radical scavenger properties of the zeolite and the potential use as a biosensor. In addition, it can also function as a reservoir for NO, an important vasodilator in artificial vascular prostheses [6].

Finally, regarding antibacterial activity, there is no doubt that some metals can be extremely toxic to most bacteria and yeast at exceptionally low concentrations, showing biocidal activity since ancient times. However, the specific mechanism to explain the toxicity of metals is not yet fully elucidated, as several factors are involved. Nevertheless, depending on the properties of the metal, the biocide behavior can be triggered by: (a) the reducing potential of the metal and (b) the atomic selectivity of the donor metal and/or speciation [30]. For Fe to function as an antimicrobial material the following ferrous iron-rich associated phases, such as pyrite (FeS_2), marcasite (FeS_2) magnetite ($FeFe_2O_4$), pyrrhotite ($Fe_{1-x}S$ where x = 0–0.2) and goethite (FeO(OH)), can act as bacteriostatic agents (inhibit growth) or by disrupting the bacterial cell wall as bactericidal agents (kill bacteria) [1].

When classified by the antimicrobial behavior four classifications are used: (1) “Trojan-horse effect” due to endocytosis processes; (2) attachment to the membrane surface via sites of adsorption for metal ions; (3) catalyzed radical formation inducing an oxidative stress; and (4) release of metal ions which can combine several of the mentioned mechanisms. The toxic mechanisms of antimicrobial materials coming from the mixture of an antimicrobial agent and a non-active material (in this case, the zeolite) are as similar as the mechanism of the agent itself. In zeolite/metal composites, the main toxic mechanism relates to the metal with two possible routes depending on the species considered as the active agent: (1) the metal particles or (2) the metal ions released from the particles. These mechanisms are revised and explained elsewhere in much more detail [31].

Furthermore, an interesting synergy has also been detected in zeolites for human bacterial pathogens, including antibiotic-resistant strains, through the synergistic actions of Fe and Al. The structural Fe^{2+}, which produces lethal hydroxyl radicals (OH), at near neutral pH and other reactive oxygen species (ROS) upon its oxidation in air, are critical too. The importance of ROS in attacking cell membranes, intercellular penetration of soluble Fe^{2+} and its subsequent oxidation to produce OH that damage intracellular proteins were found [1]. The Fenton reaction is another mechanism employing Fe^{2+}, in which the main mechanism for cell death is the degradation of intracellular critical cell components, excluding extracellular processes. In this mechanism, Fe^{2+} overcomes the regulatory proteins outside the membranes and oxidizes as soon as it enters the cell, precipitating as Fe^{3+} producing lethal hydroxyl radicals. This interpretation explains the bactericidal action of the Fe^{2+}-containing materials. Similarly, the Al^{3+} in zeolites whose ionic radius is significantly smaller than that of Fe^{2+} could replace Ca^{2+} and Mg^{2+} in the bacteria membrane, and due to the chemical affinity of Al^{3+} with phosphate ligands, it could modify lipid–protein interactions when it is bound to phospholipids. Another mechanism for Al^{3+} interferes with the membrane's electrical potential, inhibiting membrane transport proteins. Hence, the synergy of Al and Fe enhances toxicity by promoting changes and damage to the structure of bacterial membranes, increasing their permeability and oxidation [1].

Nevertheless, further understanding of the wide variety of structures of Al [32], Fe [33–36] metal sites in zeolites [37] and their dynamic properties [38,39] are needed to fully elucidate the exact antimicrobial mechanism of action of metal modified zeolites. In this study, a Y zeolite exchanged with iron was modified by a sonochemical method, and a screening experiment in an agar diffusive and a broth assay was used to evaluate and select the most promising material from the samples with antimicrobial activity. These materials were tested in clinically relevant microorganisms considering GN, GP and Fungi. The most promising materials with antimicrobial properties were further used in a broth microdilution assay to evaluate concentration effects, and a cell viability test in mouse connective tissue fibroblasts was used to measure toxicity. Finding that FAU modified with Fe by a sonochemical method can produce an antimicrobial material without toxicity in mammal cells.

Materials and Methods

This methodology is a replication of our previously published study [40] with a slight change by evaluating a different zeolite. In brief, the Fe-modified zeolite Y materials were subjected to solid and liquid antimicrobial assays (Figure 1) with strains from the American Type Culture Collection (ATCC®). The used bacteria strains were Escherichia coli (*E. coli* ATCC 25922), Enterococcus faecalis (*E. faecalis* ATCC 29212), Staphylococcus aureus (*S. aureus* ATCC 23235) and Streptococcus mutans (*S. mutans* ATCC 25175); and the fungi: Candida albicans (*C. albicans ATCC* 10231) and Cryptococcus neoformans (*C. neoformans* ATCC 90112). For agar assays, *C albicans*, *C. neoformans*, *S. aureus* and *S. mutans* were cultured on nutrient agar (Müller Hinton for bacteria and Sabouraud for fungi) for 24 h at 37 °C. Next, 4-6 colonies were selected and added to a broth culture medium (Müller Hinton for bacteria and trypticase soybean for fungi), adjusting the turbidity to 0.5 McFarland by measuring optical density at 625 nm (0.1 absorbance) by means of UV-Vis spectroscopy. To evaluate antimicrobial activity against pathogens, an agar diffusion assay was used. On a sterile Petri dish using Müller-Hinton agar (for *S. aureus* and *S. mutans)* and Sabouraud agar (for *C. albicans* and *C. neoformans)*, the microorganisms were inoculated by the lawn incubation technique. A well was made in the agar by perforating the medium with a sterile micropipette tip. Placing inside the agar well a blank disk previously immersed in a material solution of 1 mg/mL, and incubating for 24 h at 37 °C. To evaluate the bactericide activity in solids, *E. faecalis* was seeded in a CHROMagar Orientation followed by placing the immersed disks in a material solution of 1 mg/mL on the agar plate, incubating for 24 h at 37 °C, and inhibition was detected by visual inspection.

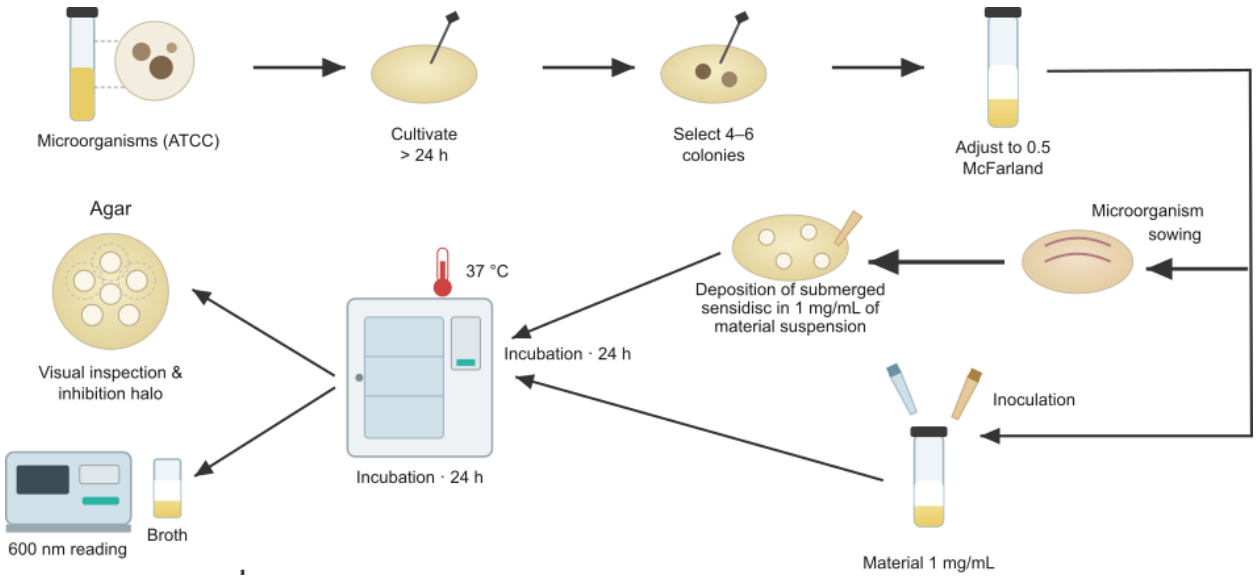

Figure 1: Procedure for antimicrobial evaluation in solid and liquid agar of Y zeolite modified by ultrasound with Fe species.

The bactericidal activity against *E. coli* (GN) and *E. faecalis* (GP) were evaluated by a broth assay, adding 4 µL of 0.5 McFarland suspension to 3 mL of Müller Hinton and mixing 1 mL of material suspension at 1 mg/mL, incubating for 48 h at 37 °C and measuring growth at 625 nm. In the same way, a microdilution experiment is carried out considering the screening, selecting two materials with the higher potential for inhibition of *E. coli* (GN) and *E. faecalis* (GP), at different material concentrations of 30, 10, 7, 2, and 1 mg/mL in Müller Hinton broth with 1 µL of 0.5 McFarland solution, incubating for 24 h at 37 °C and measuring growth at 625 nm. Finally, the antifungal activity was tested against *C. albicans* and *C. neoformans* in trypticase soybean broth under the same microdilution method.

Before the viability test (Figure 2), mouse connective tissue fibroblasts (L929) were cultured and acquired from the American Type Culture Collection (ECACC, CCL-1). These cells are derived from the first clone of the mouse L strain and are commonly used for toxicity testing in cell lines. Cells were kept in Dulbecco's Modified Eagle Medium (DMEM) supplemented with 10% fetal bovine serum (FBS) and 1% penicillin-streptomycin (PS), and were incubated under standard conditions of humidity at 37 °C and 5% carbon dioxide.

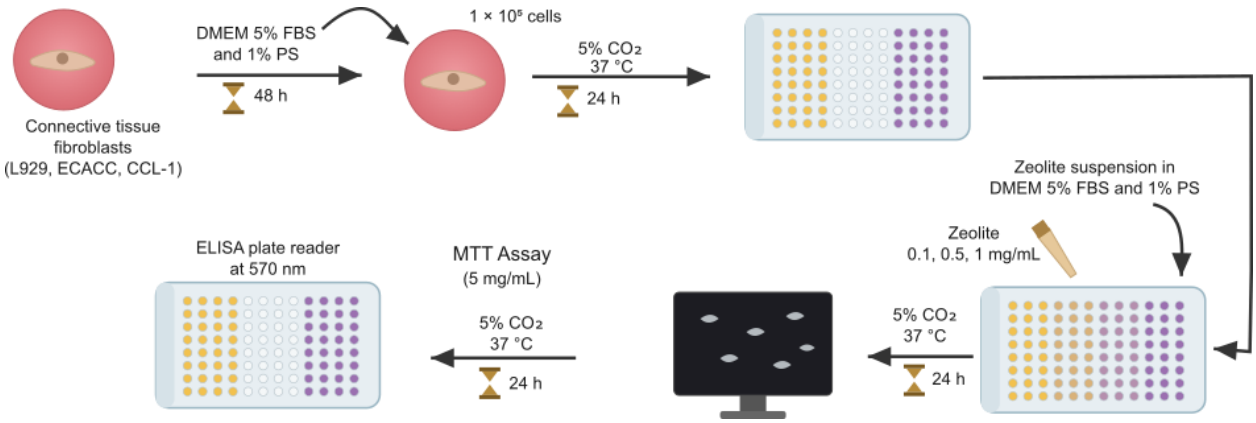

Figure 2: Procedure for measuring cell viability with the MTT assay of ultrasound-modified zeolite Y with Fe species.

Subsequently, the cells were incubated for 48 hours in DMEM supplemented with 5% FBS and 1% PS for growth. For the study, 1 ×10^5 cells were seeded in 96-well plates and pre-incubated for 24 hours before exposure to zeolites. All zeolites were discontinued prior to exposure in 20 µL of MQ water mixed with 80 µL of complete medium with 5% FBS and 1% PS. The cells were then incubated for 24 hours at 37 °C with 5% CO2 and exposed to zeolites, Y, FeYII, and FeYII/III at final concentrations of 0.1, 0.5, and 1 mg/mL. During incubation, at a 24-hour interval, microscopic images of zeolite precipitation and cell uptake compared to negative control were obtained using the Etaluma Lumascope 620 microscope with the brightfield setting and a 40× objective lens, at 1-hour time intervals for visual inspection of the cells.

The effect of exposure to the Fe modified zeolitic material on cell viability was measured using the MTT assay. After the 24-hour treatment period, 10 µL of MTT solution (5 mg/mL, Sigma-Aldrich) was added to each well and incubated for 4 hours at 37 °C with 5% CO2. Subsequently, the formazan crystals produced by the viable cells were solubilized using 100 µL of lysis solution (acidified isopropanol, MTT Kit). Finally, the plates were measured using an ELISA plate reader at 570 nm, with a baseline measurement at 690 nm. With the help of graphics software (OriginLab), feasibility graphs were constructed, comparing the results with the vehicle control (water MQ).

Results and Discussion

Disk Diffusion Antimicrobial Susceptibility Assays

The prepared materials did not inhibit growth against the pathogens of clinical interest (Figure 3), when evaluated by the antimicrobial susceptibility test in a disk-diffusion assay [41–43]. Compared to the control, no inhibition halos were detected, evidencing the lack of activity due to poor diffusion of the material through the solid agar, as expected according to the literature [22]. Meaning that these samples do not present agar-soluble, biologically active Fe species [44]. Encouraging that the antimicrobial mechanism of action is not through the release and diffusion of Fe species or ROS from the Fe-modified zeolite [31,45–47].

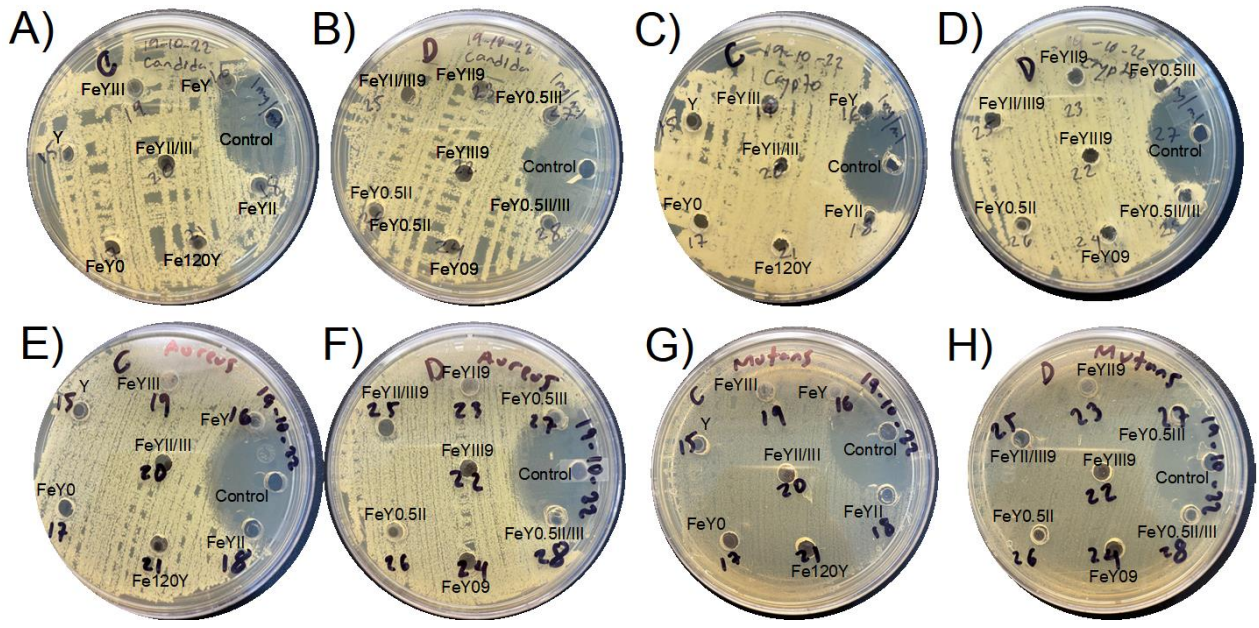

Figure 3: Antimicrobial susceptibility assay by well disk diffusion on an agar plate against the fungi A-B) *C. albicans*, C-D) and *C. neoformans*, and the bacteria E-F) *S. aureus* and G-H) *S. mutans* by immersion of a disk in a 1mg/mL sono-assisted Fe-modified zeolite Y solution.

To ensure that no diffusion from the Fe-zeolite can occur, the test was repeated with a high contrast assay, using CHROMagar Orientation with *E. faecalis* (Figure 4), which grows in bright turquoise blue colonies [48]. Showing no inhibition halo, confirming that the mechanism of action for antimicrobial is not through the release and diffusion of species from the Fe containing FAU [23]. Suggesting that the Fe species with biological activity in the prepared iron zeolites do not diffuse into the solid agar and that perhaps liquid is needed to be biologically active through the generation of ROS [46,47,49].

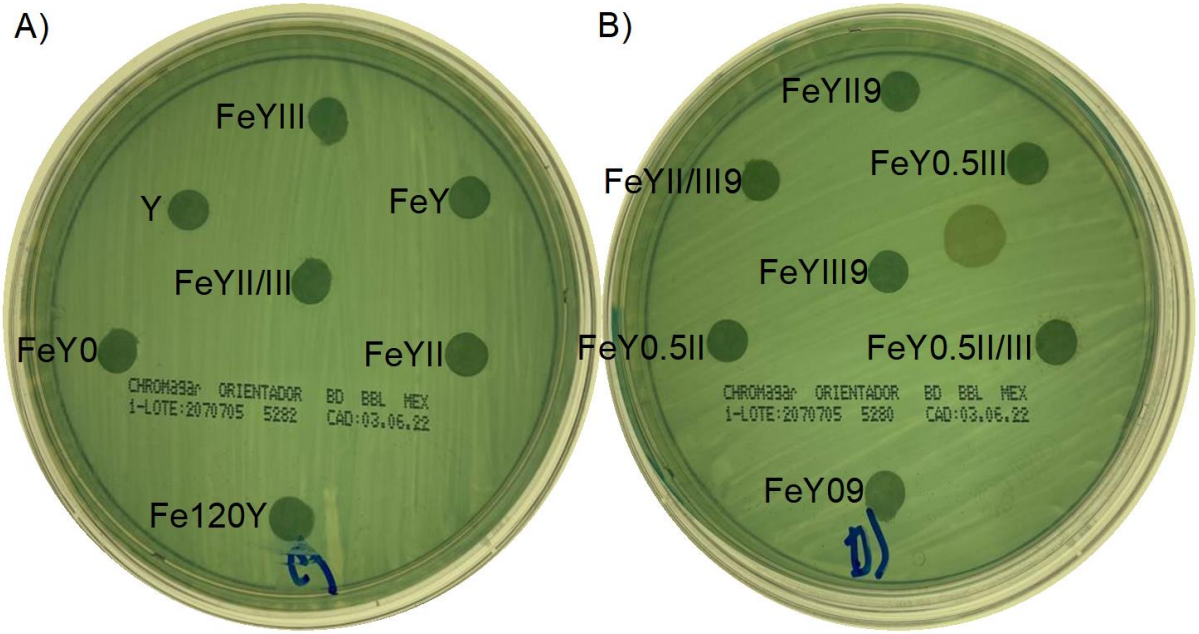

Figure 4: Antibacterial susceptibility assay by disk diffusion on an agar plate against *E. faecalis* by immersion of the disk in a 1mg/mL sono-assisted Fe-modified zeolite Y solution.

Broth Antimicrobial Susceptibility Assays

Given that the inhibition mechanism for the prepared materials is not active through the diffusion of Fe species, a broth assay was evaluated (Figure 5A), and all samples showed some antibacterial activity, including the pristine Y zeolite. For *E. coli*, FeY0, FeY0.5II, FeY0.5III, FeYII/III, and FeYII/III9 were the samples with the highest antimicrobial activity against GN bacteria, showing a bactericide effect whereas the rest presented bacteriostatic action [1,22,24,50]. A characteristic of GN bacteria is that their membranes contain more layers, with a slightly negative zeta potential (ζ=-5 mV) compared to the negative ζ (-20 mV) in GP bacteria [21], which could help us understand the type of Fe species we have in these samples. Zeolites with a negative ζ do not adsorb well on GN bacteria, compared to their adsorption to GP bacteria. Given that these sono-assisted prepared Fe-zeolites exhibit a negative ζ (-20 mV) [51], low adsorption is expected between *E. coli* and the zeolitic surface. In contrast, for *E. faecalis*, the assumed higher surface interaction can explain the bacteriostatic effect detected in all the samples, where FeY0, FeYII and Fe5Y showed bactericidal properties. Presenting three simplistic sono-assisted Fe modification pathways to prepare selective antibacterial Fe-modified zeolites. Tuning the antibacterial properties of the parent Y-type zeolite to be of wide spectrum against both GN and GP or selective against a specific bacteria cell wall type. First, the Y zeolite is subjected to an ion exchange (FeY), resulting in a material with less effect against GN and greater effect on GP bacteria. When modifying FeY with ultrasound, depending on the medium at which it is sonicated, the antimicrobial properties can be tuned to be of wide spectrum (FeY05) or selective to GN (FeYII/III5) and GP (FeYII5). If FeY is sonicated in an ammonia buffer at pH=5, without the addition

of extra Fe to the suspension (FeY05), a wide-spectrum antibacterial material is obtained. However, if Fe(II) is added to the suspension (FeYII5) the antibacterial mechanism is selective for GP. In contrast, when the suspension is spiked with Fe(II) and Fe(III), the effect shifts to be selective against GN. These simplistic modifications highlight the most effective samples and thus those with the highest potential for medical applications. According to these results, FeYII/III and FeYII showed selective bactericidal properties for *E. coli* and *E. faecalis,* respectively. Presenting a selective type of cell wall-dependent effect by only changing the ratio of Fe^{2+} and Fe^{3+} added to the Fe-Y modification solution. Hence, these were selected and tested at different concentrations in a broth microdilution assay to gain more knowledge on the possible reaction mechanism.

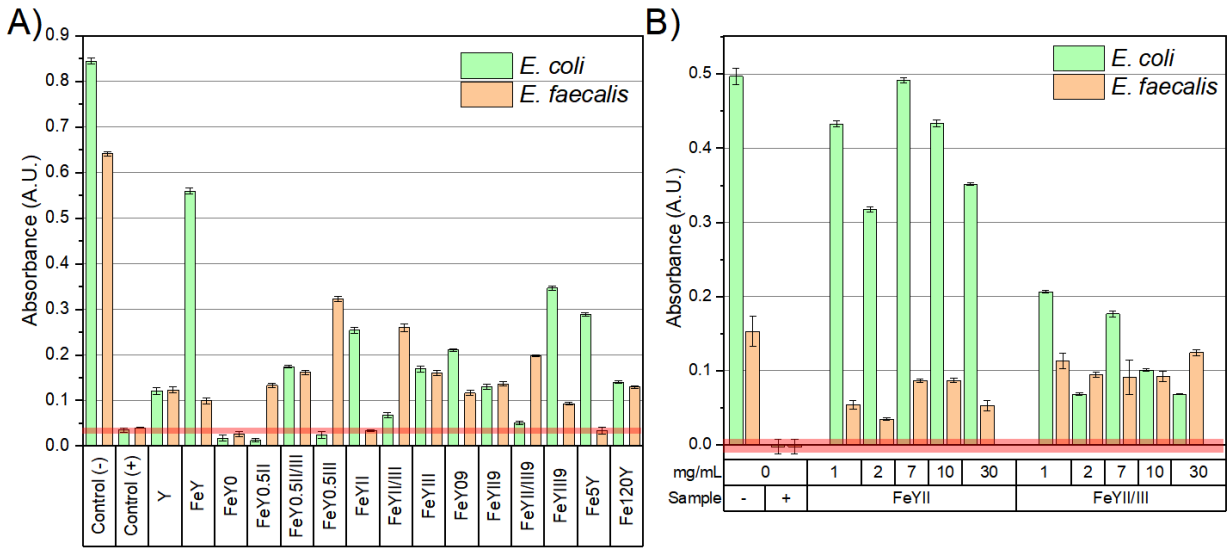

Figure 5: Antibacterial A) broth susceptibility assay against *E. coli* and *E. faecalis* in a concentration of 1mg/mL sono-assisted Fe-modified zeolite Y solution incubated for 48 h at 37 ºC and B) broth microdilution incubated for 24 h at 37 ºC at a solution concentration of FeYII and FeYII/III modified zeolites of 30, 10, 7, 2 and 1 mg/mL.

When evaluating the antibacterial properties of FeYII against *E. coli,* a bacteriostatic effect was seen at 24 h with no linear dependency between growth inhibition and concentration (Figure 5B). Given that the surface of *E. coli* is known not to absorb zeolites, excluding the attachment to the membrane surface as the main antibacterial mechanism of action. In addition, FeYII/III showed a higher bacteriostatic effect on *E. coli*, with the same non-linear trend. Meaning that increasing concentration increases the antimicrobial effect, reaffirming that compared to FeYII, FeYII/III has more selective GN antibacterial Fe species or Fe active sites. The mechanism of action of these species could play a role by acting at close proximity, regardless of the bacterial-zeolite surface interactions. Supporting the above-mentioned, the addition of Fe(II) or a mixture of Fe(II)/Fe(III) under ultrasound produces different Fe species or even different Fe sites. Likewise, comparing the higher concentration of both samples (Figure 5B), the contrasting antibacterial effect observed in the screening experiments was replicated (Figure 5A).

Different variables were found to correlate with bacterial growth from a multivariate multiple linear regression analysis (Figure 6). Highlighting the complexity of these systems for describing the multiple possible mechanisms of action. The variables with significant effect and predicting power for the growth of *E. coli* (GN), obtained from the characterizations published elsewhere [52], served to construct the following model (equation 1):

$$\text{GN Growth} = -5.39335 + (0.5617\ \text{pH}) + (0.02413\ \zeta) + (0.1964\ \alpha - \text{Fe(II)}) + (-0.00209\ \text{SI and SII'}) \quad (1)$$

where pH is the value at which the zeolite was modified, zeta potential (ζ, mV) measured in deionized water, α-Fe (II) the area detected at 570-600 nm from the deconvolution of UV-Vis diffuse reflective spectroscopy (UV-Vis DRS), and SI' and SII' the area of OH vibrations forming hydrogen bonds with water at the specified cation exchange sites (3040 cm^{-1}) from the deconvolution of the ATR FT-IR spectroscopy.

Zeolites are known not to adsorb on GN bacteria surfaces [21], explaining the antimicrobial effect of ζ through electrostatic interactions. In addition, the pH at which the zeolites are prepared and the presence of α-Fe (II) seem to have the greatest effect on the bactericide mechanism. Hinting that the mechanism against GN is a combination of a Fe-dependent and surface interaction. Adding complexity to the mechanism, the species at SI ' and SII ´cation exchange sites also play a role. It is worth mentioning that these sites are known to be the sites for α-Fe [53]. Hence, the presence of water in these cation exchange sites is also important to increase the predictive power of the model. From these variables, we can assume that the main mechanism of action is governed through an interaction of these α-Fe active sites and the amount of adsorbed water at SI' and SII' cation exchange sites. Explaining that the concentration of Fe sites, low ζ and surface adsorbed species are enough in samples FeY05 and FeYII/III5 to inhibit the growth of GN, while the higher amounts of water in SI' and SII' sites in FeYII5 repel E. coli, enabling growth.

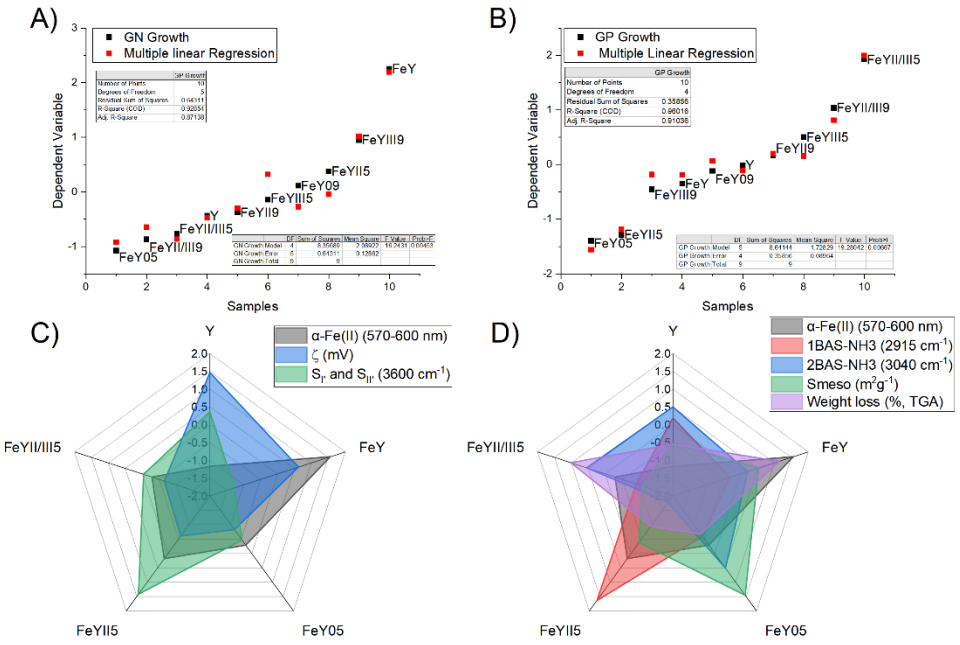

Figure 6: Multivariate multiple linear regression analysis of A) E. coli (GN) and B) E.faecalis (GP) growth and radar plot using Fe(II) measured at 570-600 nm from UV-Vis deconvolution, BAS-NH_3 , $S_{I'}$ and $S_{II'}$ from ATR FT-IR, surface ζ, mesoporous surface from physisorption and weight loss percentage (W%) from thermogravimetric analysis (TGA) data for C) GN and D) GP of a sonoassisted modified Y zeolite with iron at different oxidation numbers (ON) of divalent (II) and trivalent (III) at 1 % at pH 5 or 9.

In contrast, for predicting the growth of E. faecalis (GP), the model is more complex (equation 2):

$$\text{GP Growth} = -15.94 + (0.7640\ \text{W\%}) + (-0.0642\text{Smeso}) + (-0.0231\ \alpha - \text{Fe(II)}) + (-0.0009\ 1\text{BAS} - \text{NH3}) + (-0.0003\ 2\text{BAS} - \text{NH3}) \quad (2)$$

Where the variables with a significant effect are: α-Fe (II) (570-600 nm), NH_3 linked Bronsted acid sites (BAS-NH_3) detected at 2915 cm^{-1} (1BAS-NH_3) and 3040 cm^{-1} (2BAS-NH_3), from the deconvolution ATR-FT-IR spectra; surface area of mesopores (S_{meso}) measured from N_2 physisorption adsorption-desorption isotherms; and the weight loss percentage (W%) detected from the thermogravimetric analysis (TGA). Zeolites adsorb on the GP bacteria surface due to electrostatic interactions despite both having a net negative ζ [21], explaining why ζ was not a significant effect. Nevertheless, the weight loss percentage (denoting the loss of water and ammonia and dehydroxylation) had the most effect on GP growth in combination with the S_{meso}. Suggesting that the main mechanism is due to surface interaction. Where more surface adsorbed species such as water, ammonia and hydroxyls increase growth, a higher S_{meso} would enhance growth inhibition. Given the higher concentration of adsorbed species and lower S_{meso} in FeYII/III5, the growth of GP is favored. Similar to GN, α-Fe was also useful to produce the employed model, suggesting that this may be the mechanism responsible for the wide spectrum measured at FeY05. In addition, BAS-NH_3 also plays a role in the GP growth inhibition, adding complexity to the mechanism of action. Where FeYII5 with the most 1BAS-NH_3 exhibits the highest selectivity against GP. Supporting that the selectivity against GP is due to local bacteria-zeolite surface interactions and α-Fe species.

When inspecting the means by an ANOVA, the selective effect of each sample is more clearly illustrated. Where the growth inhibition against *E. coli is stronger with* FeYII/III, and for *E. faecalis* with FeYII (Figure 7A). A complex behavior involving more than one mechanism of action is suggested, where these mechanisms have a concentration-dependent interaction. The antimicrobial activity developed at low concentrations (<7 mg/mL) is different than those mechanisms at higher concentrations (≥ 7mg/mL). Suggesting that the mechanism of action against *E. coli* is concentration-dependent. In contrast, the activity against *E. faecalis,* although having the same trend, the antibacterial effect is more homogeneous, involving a non-concentration-dependent mechanism of action, since both FeYII and FeYII/II samples show bacteriostatic effects. Reaffirming the observation that this sonochemical method has the potential to investigate and understand different Fe sites or Fe speciation, and fine-tuning for desired applications can be achieved. These extend to catalytic and biological applications in macromolecules such as carbohydrates or broad-spectrum bactericidal agents.

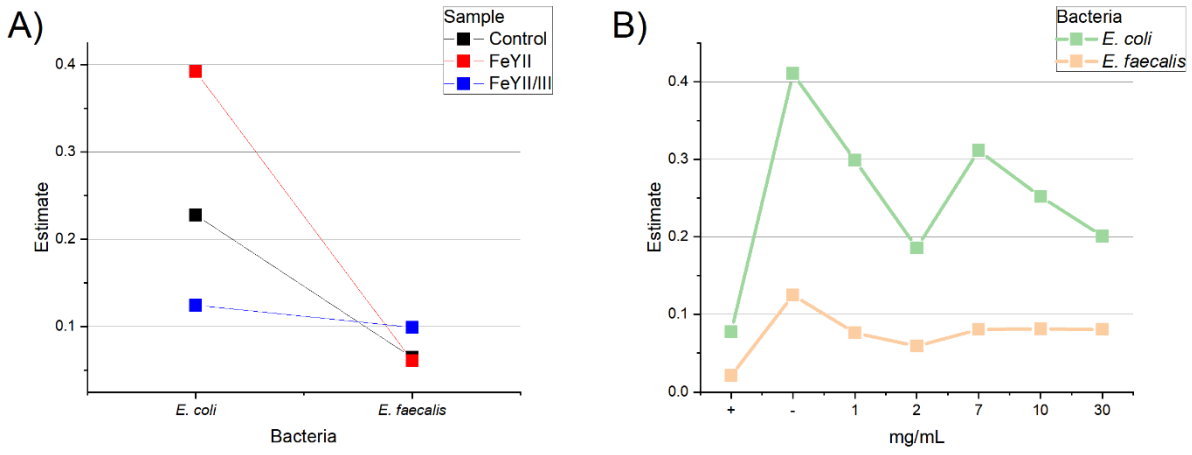

Figure 7: Means comparison plots from an ANOVA analysis for bacteria inhibition and the interaction effect of A) bacteria and materials B) and their concentrations

However, FeYII/III can inhibit the growth of bacteria with both types of cell wall, GP and GN, stating that the antimicrobial effect of this sample is attributed to multiple mechanisms of action. For *E. coli*, regardless of the employed material, the concentration has a greater effect at 2 mg/mL and 30 mg/mL (Figure 7). Meaning that the main antibacterial mechanism against *E. coli* is concentration-dependent, and that *E. faecalis* is resistant to this mechanism. For biocide metal, toxicity can be classified by the site of action, where the two usual mechanisms are the membrane surface and intracellular region, suggesting that the main mechanism occurs inside the bacterial cell [30]. Equally, increasing the concentration to 7 mg/mL lowers the efficiency of this concentration-dependent mechanism, which can be explained by the previously mentioned low *E. coli*-zeolite surface interaction. Nevertheless, the role of the cell membrane disruption can not be totally excluded. Since Fe can exhibit antimicrobial activity against a variety of pathogens, including GP, and GN bacteria and fungi, by oxidative stress and cell lysis through (a) generating ROS, (b) damaging DNA, (c) inactivating enzymes, (d) destabilizing proteins,(e) damaging ribosome,(f) impairing efflux pump, and (g) disrupting cytoplasm, and (h) cell membrane. Nonetheless, among these, four well-defined mechanisms have been postulated thus far: (i) oxidative stress by ROS generation,(ii) reduced expression of antibiotic resistance genes, protein, and enzyme deactivation, (iii) disruption of the cell wall and DNA replication, and (iv) impairment of efflux pump [47]. Suggesting that a certain spatial proximity between the zeolitic material and bacteria is needed for any of these mechanisms of action to be effective. Hence, considering that zeolites adsorb on *the E. faecalis* surface and are sensitive to a non-concentration-dependent mechanism which is active against *E. coli*. The bactericide properties of these materials are attributed to minimum three mechanisms that are dependent on: material concentration ([MC], bacteria-zeolite surface interactions (B-Zeo) and spatial proximity (SP).

Considering that in these Fe-modified zeolite Y samples, three main mechanisms ([MC], B-Zeo and SP) govern bacteria inhibition and that the inhibition of GN is concentration dependent, and that of GP is limited to surface interaction. The mechanisms relevant to biocidal activity in these samples emerge from the endocytosis of Fe-zeolite (the Trojan horse effect) and the generation of ROS, which is consistent with the four well-defined postulated mechanisms. The same profile is formed in all samples by analyzing the concentration effects (Figure 7B), increasing the toxicity from 1 to 2 mg/mL and decreasing the effect from 2 to 7 mg/mL, further increasing from 7 to 30 mg/mL. If the property of FAU as a ROS scavenger is considered, these data suggest that at low concentrations of zeolite, ROS are the main mechanism for the generation of toxic effects [7–9]. Having low amounts of ROS along with electrostatic repulsion suggests

that increasing the zeolite concentration, due to a saturation effect, local Fe-bacteria interactions would increase the likelihood of internalizing Fe species by the cell. Equally, by increasing the zeolite concentration, more ROS will be adsorbed, and thus the internalized species (ROS and Fe-species) in the cytoplasm, are more likely to cause intracellular damage, such as enzyme deactivation, cell wall rupture, and efflux pump deterioration [47].

When evaluating the antimycotic activity of selected materials against *C. albicans* and *C. neoformans*, no activity was seen from the disk diffusion assay (Figure *3*). Nevertheless, although fungi are more resistant to the mechanisms by which Fe-zeolites kill bacteria, in the microdilution assay (Figure 8), a bacteriostatic effect was detected. Considering the constant bacteriostatic effect, a non-concentration mechanism is suggested. This is explained by the main intracellular mechanism of these Fe-FAU, where they must be internalized to produce an antifungal effect. The ζ of the fungi membrane protects them from internalization due to electrostatic repulsion, given that both the fungi and the zeolitic material possess a negative ζ [54–59].

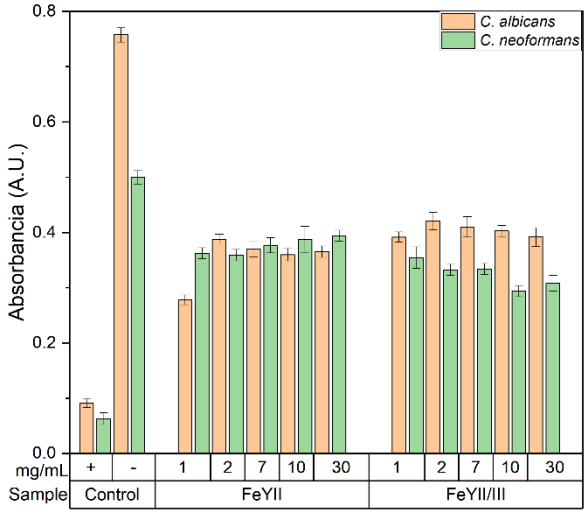

Figure 8: Antifungal broth microdilution susceptibility assay against *C. albicans* and *C. neoformans* incubated for 24 h at 37 ºC at a solution concentration of 30, 10, 7, 2 and 1mg/mL of sono-assisted Fe-modified zeolite Y (FeYII and FeYII/III).

Cell Viability Assay

When evaluating their activities against mouse fibroblasts to detect toxicity (Figure 9), the materials were non-toxic, as the cells were kept alive even at the highest concentration (1 mg/mL). However, the FeYII/III sample did show an effect at 24 hours, reducing the population to 56 %. This is not surprising since FAU is known to be biocompatible [4,6], and even though Fe could cause cell damage, it is safe at low concentrations [60], as demonstrated in this study. From the constructed video taken in the exposure experiment (Supplementary Material), the cells interact with the Fe-modified zeolite, and as time passes, the motility is reduced without affecting the original shape [61].

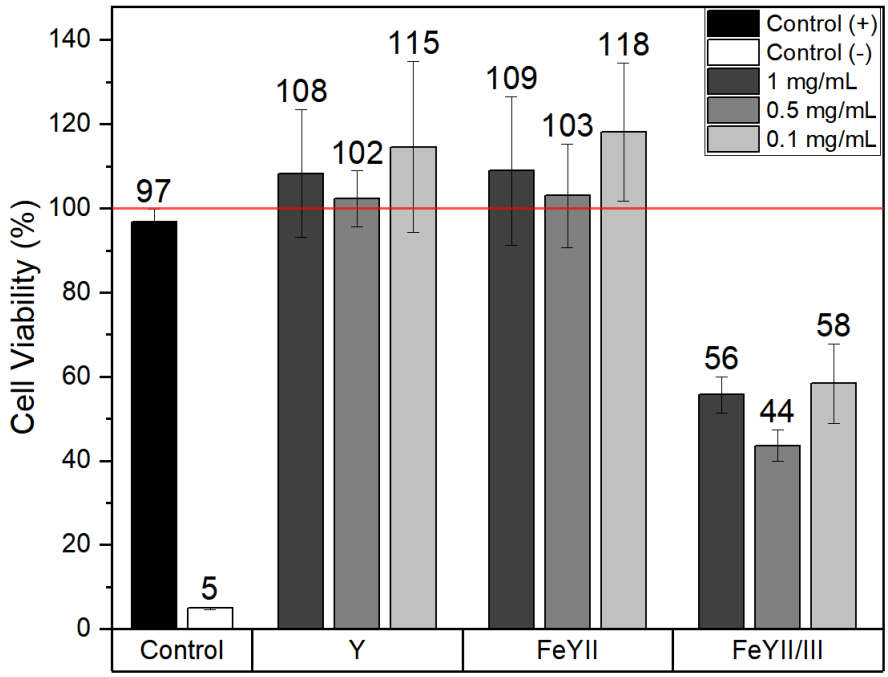

Figure 9: Cell viability measured by the MTT assay against mouse connective tissue fibroblast (L-929) for 24 h at concentrations of 0.1, 0.5 and 1mg/mL of a zeolite Y and sono-assisted Fe-modified zeolite Y (FeYII and FeYII/III).

However, in the FeYII/III sample, we see an increase in motility and a more dynamic spindle morphology, with evidence of filopodia and lamellipodia-like extensions [62]. Although some rounded cells were detected, which are attributed to slower proliferation rates [63], the majority were highly motile, spindle-shaped. In addition, the FeYII/III sample is where the least viable cells are detected (44%), explained by a slowing of their proliferation rate. Suggesting that this FeYII/III sample may be toxic to mammalian connective tissue cells [64]. Nevertheless, we must highlight that these FeYII/III particles are bioactive and can interact with fibroblasts. More studies are needed to prove that they are not harmful to the human body and that these materials serve in biomedical applications. Hence, further studies should consider Fe-modified zeolites as candidates for biological applications, including humans, given that these were found to be non-toxic.

In the future development of methods that employ Fe-modified zeolitic materials in biological systems, the speciation of Fe in these samples should be considered. With a change as small as the molar ratio of FeII: FeIII, from 1:0 to 1:1 (maintaining the 1% wt of Fe), decreased cell viability to almost 50%. This implies that the preparation and tuning of Fe species is sensitive and that sonochemical techniques can assist in the selective Fe-modification of zeolites. This sono-assisted methodology can assist in the synthesis of potential toxic Fe species or enhance interspecies mechanisms for the interaction of the Fe-modified zeolite and cells. Given the above-mentioned complexity, the ultrasonic synthesis technique is believed to have great potential for the preparation, tuning and study of iron species in zeolites.

Conclusions

In this study we show that sonoassisted Fe-modified zeolite Y represents a promising antimicrobial material whose selectivity and biocompatibility can be finely tuned depending on the FeII:FeIII ratio and modification conditions. From the tested materials, FeYII/III exhibits bactericidal activity against *E. coli*

(Gram-negative), while FeYII against *E. faecalis* (Gram-positive). Highlighting the ability to tune antibacterial selectivity via the employed sonochemical treatments with different Fe oxidation state ratios. Nonetheless, the disk-diffusion assay showed no inhibition in solid agar, due to solid-phase diffusion limitations. Testing in broth confirmed that antimicrobial action requires liquid media and likely close spatial proximity or internalization of Fe-zeolite. Finding that for predicting the activity against *E. coli*, α-Fe(II) sites, ζ and the SI'/SII' are useful. Whereas for *E.faecalis*, α-Fe(II) sites, mesoporosity, and adsorbed water/ammonia are driving bacterial inhibition. Evidencing that multiple antimicrobial pathways likely operate in tandem involving ROS generation, Fenton-related reactions, and potential Trojan-horse cellular uptake.

When evaluating cell viability, pristine Y and FeYII proved non-toxic toward L929 fibroblasts, even at 1 mg/mL (the highest concentration evaluated). In contrast, FeYII/III reduced viability to ~44–58% after 24 hours. The biocompatibility of FeYII points toward safe biomedical use, while FeYII/III is cytotoxic at higher doses. Suggesting that toxic effects can arise from specific Fe speciation or internalized species despite the overall biocompatibility of FAU zeolites. Cytotoxicity testing was limited to one fibroblast line; long-term cell and in vivo studies are needed. As well as, extended biocompatibility assays across diverse mammalian cell lines, and implement in vivo toxicity and antimicrobial efficacy testing. This shows that the technique by which zeolites were modified is sensitive to the preparation of Fe species and that there are species that are toxic and/or mechanisms between species that could benefit or affect cells.

The ultrasonic synthesis approach offers a powerful route for tuning iron-zeolite materials with controlled antimicrobial performance and cell compatibility. This technique shows promise for preparing and studying iron species due to its complexity. Opening routes for applications such as wound dressings, antimicrobial coatings, or drug-delivery matrices provided further optimization and safety validations. Likewise, for the future use of these materials in biological systems, the speciation of Fe in these samples should be considered.

Acknowledgments

Víctor Alfredo Reyes Villegas acknowledge SECIHTI for providing a doctoral scholarship and Jesus Isaias De Leon Ramirez for the postdoctoral fellowship BP-PM20250912153102760-13358161. This work was supported by the National Autonomous University of Mexico (UNAM) through supercomputer time in the LANCAD-UNAM-DGTIC-423 and 084 projects, as well as resources provided by the projects from SECIHTI CBF-2025-G-470, PAPIIT-DGAPA-UNAM IG101623 and the Russian Federation represented by the Ministry of Science and Higher Education of Russia through the agreement no. 075-15-2025-661, dated August 25, 2025. Also important was the support of the academic staff and especially of Dr. Miguel Ángel Hernández-Espinosa from the Department of Zeolite Research, Institute of Sciences, Meritorious Autonomous University of Puebla (ICUAP-BUAP).

References

(1) Gomes, C. F.; Gomes, J. H.; da Silva, E. F. *Environ. Geochem. Health* **2020**, *42*, 3507–3527. doi:10.1007/s10653-020-00628-w

(2) Mallette, A. J.; Shilpa, K.; Rimer, J. D. *Chem. Rev.* **2024**, *124*, 3416–3493. doi:10.1021/acs.chemrev.3c00801

(3) Baerlocher Christian; McCusker Lynne B.; Olson David H. *Atlas of Zeolite Framework Types*; Elsevier, 2007; Vol. 6. doi:10.1016/B978-0-444-53064-6.X5186-X

(4) Serati-Nouri, H.; Jafari, A.; Roshangar, L.; Dadashpour, M.; Pilehvar-Soltanahmadi, Y.; Zarghami, N. Biomedical Applications of Zeolite-Based Materials: A Review. *Materials Science and Engineering C*. Elsevier Ltd November 1, 2020. doi:10.1016/j.msec.2020.111225

(5) Li, W.; Chai, Y.; Wu, G.; Li, L. *J. Phys. Chem. Lett.* **2022**, *13*, 11419–11429. doi:10.1021/acs.jpclett.2c02969

(6) Bacakova, L.; Vandrovcova, M.; Kopova, I.; Jirka, I. *Biomater. Sci.* **2018**, *6*, 974–989. doi:10.1039/C8BM00028J

(7) Thomassen, L. C. J.; Napierska, D.; Dinsdale, D.; Lievens, N.; Jammaer, J.; Lison, D.; Kirschhock, C. E. A.; Hoet, P. H.; Martens, J. A. *Nanotoxicology* **2012**, *6*, 472–485. doi:10.3109/17435390.2011.587901

(8) Pellegrino, P.; Mallet, B.; Delliaux, S.; Jammes, Y.; Guieu, R.; Schäf, O. *Biochem. Biophys. Res. Commun.* **2011**, *410*, 478–483. doi:10.1016/j.bbrc.2011.06.002

(9) Shen, B.; Scaiano, J. C.; English, A. M. *Photochem. Photobiol.* **2006**, *82*, 5. doi:10.1562/2005-05-29-RA-551

(10) Souza, I.; García-Villén, F.; Viseras, C.; Pergher, S. *Pharmaceutics* **2023**, *15*, 1352. doi:10.3390/pharmaceutics15051352

(11) Costa, R.; Ribeiro, C.; Lopes, A. C.; Martins, P.; Sencadas, V.; Soares, R.; Lanceros-Mendez, S. *J. Mater. Sci. Mater. Med.* **2013**, *24*, 395–403. doi:10.1007/s10856-012-4808-y

(12) Seifu, D. G.; Isimjan, T. T.; Mequanint, K. *Acta Biomater.* **2011**, *7*, 3670–3678. doi:10.1016/j.actbio.2011.06.010

(13) Andersson, L. I. M.; Eriksson, H. *Scand. J. Immunol.* **2007**, *66*, 52–61. doi:10.1111/j.1365-3083.2007.01948.x

(14) Vilaça, N.; Gallo, J.; Fernandes, R.; Figueiredo, F.; Fonseca, A. M.; Baltazar, F.; Neves, I. C.; Bañobre-López, M. *J. Mater. Chem. B* **2019**, *7*, 3351–3361. doi:10.1039/C9TB00078J

(15) Angiolini, L.; Cohen, B.; Douhal, A. *Int. J. Mol. Sci.* **2019**, *20*, 2859. doi:10.3390/ijms20122859

(16) Khodaverdi, E.; Soleimani, H. A.; Mohammadpour, F.; Hadizadeh, F. *Chem. Biol. Drug Des.* **2016**, *87*, 849–857. doi:10.1111/cbdd.12716

(17) Karavasili, C.; Amanatiadou, E. P.; Kontogiannidou, E.; Eleftheriadis, G. K.; Bouropoulos, N.; Pavlidou, E.; Kontopoulou, I.; Vizirianakis, I. S.; Fatouros, D. G. *Int. J. Pharm.* **2017**, *528*, 76–87. doi:10.1016/j.ijpharm.2017.05.061

(18) Vilaça, N.; Amorim, R.; Machado, A. F.; Parpot, P.; Pereira, M. F. R.; Sardo, M.; Rocha, J.; Fonseca, A. M.; Neves, I. C.; Baltazar, F. *Colloids Surf. B Biointerfaces* **2013**, *112*, 237–244. doi:10.1016/j.colsurfb.2013.07.042

(19) Spanakis, M.; Bouropoulos, N.; Theodoropoulos, D.; Sygellou, L.; Ewart, S.; Moschovi, A. M.; Siokou, A.; Niopas, I.; Kachrimanis, K.; Nikolakis, V.; Cox, P. A.; Vizirianakis, I. S.; Fatouros, D. G. *Nanomedicine* **2014**, *10*, 197–205. doi:10.1016/j.nano.2013.06.016

(20) Abasian, P.; Radmansouri, M.; Habibi Jouybari, M.; Ghasemi, M. V.; Mohammadi, A.; Irani, M.; Jazi, F. S. *Int. J. Biol. Macromol.* **2019**, *121*, 398–406. doi:10.1016/j.ijbiomac.2018.09.215

(21) Kubota, M.; Nakabayashi, T.; Matsumoto, Y.; Shiomi, T.; Yamada, Y.; Ino, K.; Yamanokuchi, H.; Matsui, M.; Tsunoda, T.; Mizukami, F.; Sakaguchi, K. *Colloids Surf. B Biointerfaces* **2008**, *64*, 88–97. doi:10.1016/j.colsurfb.2008.01.012

(22) Daou, T. J.; Dos Santos, T.; Nouali, H.; Josien, L.; Michelin, L.; Pieuchot, L.; Dutournie, P. *Molecules* **2020**, *25*, 3414. doi:10.3390/molecules25153414

(23) Chen, S.; Popovich, J.; Zhang, W.; Ganser, C.; Haydel, S. E.; Seo, D. K. *RSC Adv.* **2018**, *8*, 37949–37957. doi:10.1039/C8RA06556J

(24) Zeeshan, M.; Nazir, R.; Tahir, L.; Alam, S.; Saleem, A.; Khan, S. A.; Zia-ur-Rehman, M. *Desalination Water Treat.* **2017**, *93*, 120–130. doi:10.5004/dwt.2017.21486

(25) Ligaj, M.; Tichoniuk, M.; Cierpiszewski, R.; Foltynowicz, Z. *Coatings* **2020**, *10*. doi:10.3390/coatings10020156

(26) Mmelesi, O. K.; Masunga, N.; Kuvarega, A.; Nkambule, T. T.; Mamba, B. B.; Kefeni, K. K. Cobalt Ferrite Nanoparticles and Nanocomposites: Photocatalytic, Antimicrobial Activity and Toxicity in Water Treatment. *Materials Science in Semiconductor Processing*. Elsevier Ltd March 1, 2021. doi:10.1016/j.mssp.2020.105523

(27) Jahangirian, H.; Rafiee-Moghaddam, R.; Jahangirian, N.; Nikpey, B.; Jahangirian, S.; Bassous, N.; Saleh, B.; Kalantari, K.; Webster, T. J. *Int. J. Nanomedicine* **2020**, *15*, 1005–1020. doi:10.2147/IJN.S231679

(28) Chen, S.; Popovich, J.; Zhang, W.; Ganser, C.; Haydel, S. E.; Seo, D. K. *RSC Adv.* **2018**, *8*, 37949–37957. doi:10.1039/C8RA06556J

(29) Ligaj, M.; Tichoniuk, M.; Cierpiszewski, R.; Foltynowicz, Z. *Coatings* **2020**, *10*. doi:10.3390/coatings10020156

(30) Palza, H. Antimicrobial Polymers with Metal Nanoparticles. *International Journal of Molecular Sciences*. MDPI AG January 19, 2015, pp 2099–2116. doi:10.3390/ijms16012099

(31) Palza, H. Antimicrobial Polymers with Metal Nanoparticles. *International Journal of Molecular Sciences*. MDPI AG January 19, 2015, pp 2099–2116. doi:10.3390/ijms16012099

(32) Ravi, M.; Sushkevich, V. L.; van Bokhoven, J. A. *Nat. Mater.* **2020**, *19*, 1047–1056. doi:10.1038/s41563-020-0751-3

(33) Maier, S. M.; Jentys, A.; Janousch, M.; van Bokhoven, J. A.; Lercher, J. A. *The Journal of Physical Chemistry C* **2012**, *116*, 5846–5856. doi:10.1021/jp300349q

(34) Li, G.; Pidko, E. A. The Nature and Catalytic Function of Cation Sites in Zeolites: A Computational Perspective. *ChemCatChem*. Wiley Blackwell January 9, 2019, pp 134–156. doi:10.1002/cctc.201801493

(35) Wang, Y.; Wang, J.; Wei, J.; Wang, C.; Wang, H.; Yang, X. *Catal. Letters* **2023**, *153*, 3311–3332. doi:10.1007/s10562-022-04238-2

(36) Snyder, B. E. R.; Bols, M. L.; Schoonheydt, R. A.; Sels, B. F.; Solomon, E. I. *Chem. Rev.* **2018**, *118*, 2718–2768. doi:10.1021/acs.chemrev.7b00344

(37) Zhang, Q.; Gao, S.; Yu, J. Metal Sites in Zeolites: Synthesis, Characterization, and Catalysis. *Chemical Reviews*. American Chemical Society May 10, 2023, pp 6039–6106. doi:10.1021/acs.chemrev.2c00315

(38) Hu, Z.-P.; Han, J.; Wei, Y.; Liu, Z. *ACS Catal.* **2022**, *12*, 5060–5076. doi:10.1021/acscatal.2c01233

(39) Krause, S.; Hosono, N.; Kitagawa, S. *Angew. Chem. Int. Ed.* **2020**, *59*, 15325–15341. doi:10.1002/anie.202004535

(40) De León-Ramírez, J. I.; Reyes Villegas, V. A.; Pérez-Sicairos, S.; Chávez Méndez, J. R.; Chávez-Rivas, F.; Yocupicio-Gaxiola, R. I.; Petranovskii, V. *PLoS One* **2025**, *20*, e0324997. doi:10.1371/journal.pone.0324997

(41) Kim, H.-E.; Liu, Y.; Dhall, A.; Bawazir, M.; Koo, H.; Hwang, G. *Front. Cell. Infect. Microbiol.* **2021**, *10*. doi:10.3389/fcimb.2020.623980

(42) Kriegl, L.; Egger, M.; Boyer, J.; Hoenigl, M.; Krause, R. *Clinical Microbiology and Infection* **2024**. doi:10.1016/j.cmi.2024.03.006

(43) Mayer, F. L.; Kronstad, J. W. *Journal of Fungi* **2019**, *5*, 31. doi:10.3390/jof5020031

(44) Schiefer, H. G.; Von Graevenitz, A. *Clinical Microbiology*; 2006. doi:10.1007/3-540-33713-X_74

(45) Lemire, J. A.; Harrison, J. J.; Turner, R. J. *Nat. Rev. Microbiol.* **2013**, *11*, 371–384. doi:10.1038/nrmicro3028

(46) Yang, X.; Yu, Q.; Gao, W.; Tang, X.; Yi, H.; Tang, X. *Ceram. Int.* **2022**, *48*, 34148–34168. doi:10.1016/j.ceramint.2022.08.249

(47) Tasnim, N. T.; Ferdous, N.; Rumon, Md. M. H.; Shakil, M. S. *ACS Omega* **2024**, *9*, 16–32. doi:10.1021/acsomega.3c06323

(48) Singh, A. K.; Bhunia, A. K. *Microb. Biotechnol.* **2016**, *9*, 127–135. doi:10.1111/1751-7915.12323

(49) Mubeen, B.; Ansar, A. N.; Rasool, R.; Ullah, I.; Imam, S. S.; Alshehri, S.; Ghoneim, M. M.; Alzarea, S. I.; Nadeem, M. S.; Kazmi, I. *Antibiotics* **2021**, *10*, 1473. doi:10.3390/antibiotics10121473

(50) Behin, J.; Shahryarifar, A.; Kazemian, H. *Chem. Eng. Technol.* **2016**, *39*, 2389–2403. doi:10.1002/ceat.201600380

(51) Reyes Villegas, V. A.; De León Ramirez, J. I.; Perez-Sicairos, S.; Yocupicio-Gaxiola, R. I.; González-Torres, V.; Petranovskii, V. *Environmental Advances* **2024**, *15*, 100475. doi:10.1016/j.envadv.2023.100475

(52) Reyes Villegas, V. A.; De León Ramirez, J. I.; Pérez-Cabrera, L.; Pérez-Sicairos, S.; Yocupicio-Gaxiola, R. I.; Chávez-Méndez, J. R.; Huerta-Arcos, L.; Petranovskii, V. *Mater. Chem. Phys.* **2025**, *331*, 130199. doi:10.1016/j.matchemphys.2024.130199

(53) Bols, M. L.; Hallaert, S. D.; Snyder, B. E. R.; Devos, J.; Plessers, D.; Rhoda, H. M.; Dusselier, M.; Schoonheydt, R. A.; Pierloot, K.; Solomon, E. I.; Sels, B. F. *J. Am. Chem. Soc.* **2018**, *140*, 12021–12032. doi:10.1021/jacs.8b05877

(54) Yu, Q.; Li, J.; Zhang, Y.; Wang, Y.; Liu, L.; Li, M. *Sci. Rep.* **2016**, *6*, 26667. doi:10.1038/srep26667

(55) Hu, S.; Gu, F.; Chen, M.; Wang, C.; Li, J.; Yang, J.; Wang, G.; Zhou, Z.; Yang, Y. *Sci. Rep.* **2020**, *10*, 12480. doi:10.1038/s41598-020-68978-0

(56) Aguiar, F. L. L. de; Santos, N. C.; de Paula Cavalcante, C. S.; Andreu, D.; Baptista, G. R.; Gonçalves, S. *Int. J. Mol. Sci.* **2020**, *21*, 8339. doi:10.3390/ijms21218339

(57) Elgiddawy, N.; Ren, S.; Ghattas, W.; Rouby, W. M. A. El; El-Gendy, A. O.; Farghali, A. A.; Yassar, A.; Korri-Youssoufi, H. *Sensors* **2021**, *21*, 1715. doi:10.3390/s21051715

(58) Hu, S.; Gu, F.; Chen, M.; Wang, C.; Li, J.; Yang, J.; Wang, G.; Zhou, Z.; Yang, Y. *Sci. Rep.* **2020**, *10*, 12480. doi:10.1038/s41598-020-68978-0

(59) Ferreira, G. F.; dos Santos Pinto, B. L.; Souza, E. B.; Viana, J. L.; Zagmignan, A.; dos Santos, J. R. A.; Santos, Á. R. C.; Tavares, P. B.; Denadai, Â. M. L.; Monteiro, A. S. *Mycopathologia* **2016**, *181*, 799–806. doi:10.1007/s11046-016-0054-z

(60) Reddy, L. H.; Arias, J. L.; Nicolas, J.; Couvreur, P. *Chem. Rev.* **2012**, *112*, 5818–5878. doi:10.1021/cr300068p

(61) Jahangirian, H.; Rafiee-Moghaddam, R.; Jahangirian, N.; Nikpey, B.; Jahangirian, S.; Bassous, N.; Saleh, B.; Kalantari, K.; Webster, T. J. *Int. J. Nanomedicine* **2020**, *Volume 15*, 1005–1020. doi:10.2147/IJN.S231679

(62) Teparat-Burana, T.; Onsiri, N.; Jantarat, J. *J. Investig. Clin. Dent.* **2017**, *8*. doi:10.1111/jicd.12177

(63) Folkman, J.; Moscona, A. *Nature* **1978**, *273*, 345–349. doi:10.1038/273345a0

(64) Jiang, L.; Qi, Y.; Kong, X.; Wang, R.; Qi, J.; Lin, F.; Cui, X.; Liu, Z. *Front. Cell Dev. Biol.* **2021**, *9*. doi:10.3389/fcell.2021.660316